Journal of Magnetism and Magnetic Materials 340 (2013) 23–26

Contents lists available at SciVerse ScienceDirect

Journal of Magnetism and Magnetic Materials

journal homepage: www.elsevier.com/locate/jmmm

Design of nanostrip magnonic crystal waveguides with a single magnonic band gap

Qi Wang [a], Zhiyong Zhong [a,*], Lichuan Jin [a], Xiaoli Tang [a], Feiming Bai [a], Huaiwu Zhang [a], Geoffrey S.D. Beach [b]

[a] State Key Laboratory of Electronic Thin Films and Integrated Devices, University of Electronic Science and Technology of China, Chengdu 610054, China
[b] Department of Materials Science and Engineering, Massachusetts Institute of Technology, MA 02139, USA

ARTICLE INFO

Article history:
Received 9 August 2012
Received in revised form
25 October 2012
Available online 28 March 2013

Keywords:
Magnonic band gap
Spin wave
Magnonic crystal
Magnetic nanostructure

ABSTRACT

A novel planar structure of magnonic-crystal waveguide (MCW) with periodic rectangular-shaped holes embedded in a magnetic nanostrip film was designed. The effects of the distance between rectangular-shaped holes in the width direction of MCW on magnonic band structures were studied by micromagnetic simulations. The results show that a MCW with a single magnonic band gap can be obtained by adjusting the distance to meet the condition of Bragg reflection of spin waves in the width direction of MCW. Moreover, the center frequency and width of magnonic gap can be regulated by changing the period and length of rectangular-shaped holes.

1. Introduction

Spin waves (SWs), which are the collective precessional motions of individual spins, have attracted scientific interest for a long time [1,2]. Earlier research focused on SWs in low loss single crystal yttrium iron garnet films [3,4]. However, in recent years, SWs in nanomagnetic structures and magnonic crystals have stimulated interest because these SWs have shorter wavelengths than that of electromagnetic waves with the same frequency. Magnonic nanodevices based on magnonic crystals are therefore promising candidates for the miniaturization of microwave devices. MCW with controllable magnonic band gaps has great potential applications in magnonic devices, such as microwave filters [5–9], logic devices [10–12], and transducers [13]. Kim et al. [5,6] studied the physical origin and generic control of magnonic band gaps of dipole-exchange SWs in width-modulated nanostrip waveguides and designed a broadband SWs band-pass filter which consisted of serial combinations of various width modulations with different periodicities and motifs in planar-patterned thin-film nanostrips. Ma et al. [7–9] investigated the propagation of SWs in different material MCW. In these studies, several magnonic band gaps coexisted in the MCW. If MCW with a single band gap can be obtained, it will enable the design of SW-based signal transmission and processing devices, such as SW band-rejection filter.

In this paper, on the basis of previous studies [5–9], a simple planar-patterned film waveguide which can be used for a gigahertz-range SW band-rejection filter with single magnonic band gap was designed. This MCW was composed simply of various periodic rectangular-shaped holes in a nanostrip and made from a single soft magnetic material [e.g., permalloy (Py)]. The origin of the resulting magnonic band gaps and their relation to the size of rectangular-shaped holes were investigated by micromagnetic numerical calculations and analytical calculations. In our simulation, a planar-patterned film waveguide on the nano-scale size was investigated due to the limit of computational capabilities. However, the results of simulation coincide with the analytical results, suggesting that the same phenomena could likewise be engineered on the sub-micrometer [14] or micrometer [15] scale size's waveguide.

2. Model and simulation method

Fig. 1 shows the schematics of a 1500 nm × 30 nm MCW with 10 nm thickness. The entire MCW structure was composed of two parts. One end of the waveguide was comprised of a strip [the dark brown and yellow area in Fig. 1], which was used to excite and propagate SWs. This strip was joined with the MCW, consisting of periodic rectangular-shaped holes with period P1 and width 3 nm, as illustrated in Fig. 1. Simulations were performed using the object oriented micromagnetic framework (OOMMF) [16] to solve the Landau–Lifshitz–Gilbert equation. In our study, in order to obtain the uniform initial state, a strong enough field was employed to technically saturate the sample along the longitudinal direction of

* Corresponding author. Tel: +86 28 83201440; fax: +86 28 83201810.
E-mail addresses: zzy@uestc.edu.cn, zyzhonguestc@yahoo.com.cn (Z. Zhong).

0304-8853/$ - see front matter © 2013 Elsevier B.V. All rights reserved.
http://dx.doi.org/10.1016/j.jmmm.2013.03.017

the waveguide. Following saturation, the field was gradually reduced to zero, however, the magnetization remained aligned in the longitudinal direction due to the shape anisotropy. The material parameters correspond to Py and the procedure used for exciting SWs were same as the references [5,6,17].

3. Results and discussion

We explore how the distance between the edge of the waveguide and the rectangular-shaped holes influences the magnonic band structure. The frequency spectra and dispersion curves for SWs propagating along the x axis are plotted in Fig. 2(a). These results were obtained by the fast Fourier transforms (FFTs) with Chebyshev window [17] of the temporal M_z/M_s oscillations in the waveguides of $d=3$ nm, 6 nm, and 9 nm. All of the dispersion curves show that the intrinsic forbidden bands below 14 GHz due to the nanostrip-width confinement [5,18]. For $d=3$ nm and 9 nm, two additional forbidden bands are observed, the higher band gap is $\Delta_g{}^h=6$ GHz and the lower band gap is $\Delta_g{}^l=10.5$ GHz. It is interesting to note that for $d=6$ nm, only one forbidden gap is observed with the band gap of $\Delta_g=10.5$ GHz. The characteristic with only one band gap is specially needed for designing band-rejection filters.

The dispersion curves of the SWs modes in the MCW with $d=3$ nm are shown in Fig.2(b). The periodic character of the dispersion spectra is calculated up to the second Brillouin zone. As seen from Fig. 2(b), the lower band gap occurs at the first Brillion zone boundaries (black dashed line), due to the periodic modulation of the rectangular-shaped holes along the SWs propagation direction [5,19]. In contrast, the higher band gap is observed at $k_x=(2n+1)/P\pm0.05$ nm^{-1}(red dashed lines), caused by the interactions between the initial lowest mode ($m=1$) and the higher width mode ($m=3$) [5,19]. For $d=6$ nm, the second band gap is disappeared obviously.

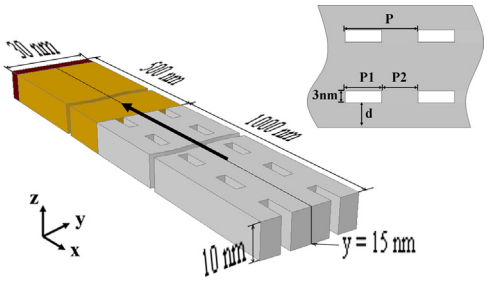

Fig. 1. Schematic of MCW with rectangular-shaped holes. The black arrow represents equilibrium magnetization. (For interpretation of the references to color in this figure, the reader is referred to the web version of this article.)

In order to elucidate the physical origin of the single magnonic band gap, we assumed a sinusoidal mode profile in the y direction, as schematically displayed in Fig. 3(b). This leads to an overall spatial distribution of the amplitude of the dynamic magnetization associated with the nth mode that can be written as

$$\psi_n(x,y,t)=A_n\sin\left(\frac{n\pi}{w_{eff}}y\right)\cos(k_x^n x-\omega t+\varphi_n) \tag{1}$$

where A_n is the maximum amplitude of the nth mode, $\omega=2\pi f$ is the cyclic excitation frequency, $k_x{}^n$ is the longitudinal wave number of the nth SW mode corresponding to this frequency, and φ_n is the excitation phase. The spatial distributions of magnetization calculated using Eq. (1) for different time are shown in Fig. 3(a) [20]. It can be observed that the third mode SW traveling along the width and longitudinal direction. The wave vector in the y direction is quantized according to $k_{m,y}=m\pi/w_{\rm eff}$ ($m=1, 2, 3, \ldots$), where m is the mode number. For the third mode ($m=3$), the wavelength in the y direction is fixed. In this geometry, the demagnetizing fields lead to an increase of the effective quantization width w_{eff}, which is larger than the geometrical width w of the strip [21,22]. Taking into account only the dipole–dipole interaction, the effective width of the strip [21,22] is

$$w_{eff}=\frac{wd(p)}{d(p)-2} \tag{2}$$

$$d(p)=\frac{2\pi}{p[1+2\ln(1/p)]} \tag{3}$$

where $p=l/w$, l is the thickness of the strip and w is the geometrical width of the strip. The wavelength in the y direction (λ_y) can be calculated, i.e. $\lambda_y=2/3w_{\rm eff}\approx30$ nm. For $d=6$ nm, the distance between the two rectangular-shaped holes is 15 nm, which equals half-wavelength of SW in the y direction. This situation meets the condition of a maximum reflectivity for Bragg reflection. The interference between the initially propagating forward mode and its backward mode reflected at the BZ boundary in the y direction leads to the result that the SW of the third mode become weaken or disappeared. The destructive interference of the third mode in the y direction, therefore, reduces the interaction between the lowest

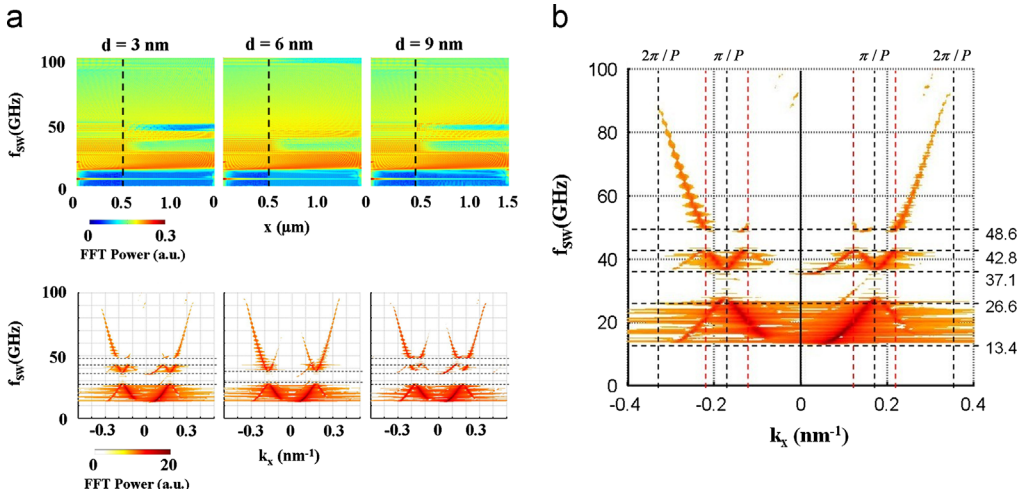

Fig. 2. (a) Comparisons of frequency spectra (top) and dispersion curves (bottom) for a 30 nm wide nanostrip and the length of rectangular-shaped holes $P1=9$ nm, the period of $P=18$ nm, with different d values. (b) Dispersion curves of SWs in the film waveguide of [$P1$, $P2$]=[9 nm, 9 nm] and $d=3$ nm. (For interpretation of the references to color in this figure, the reader is referred to the web version of this article.)

mode ($m=1$) and the third mode ($m=3$) in the x direction. As a result, the second forbidden band disappeared. According to the above analysis, different geometrical widths of strips have been checked. The second forbidden band can be shielded, only if the distance between the two rectangular-shaped holes is equal to half-wavelength of SW in the y direction.

In order to design the SW reject filter with only one forbidden band in a wide frequency range, the width of the band gap that appears at the first BZ boundary was studied. It can be understood that the Bragg reflection in MCW arises due to the inhomogeneous demagnetizing field between the rectangular-shaped holes. This behavior motivates an analytical model to estimate the band gaps, in analogy to the well-known case of Bragg reflection of electrons in a periodic potential [23,24].

$$\Delta\upsilon_k \approx \frac{\gamma}{2\pi}\sqrt{2|H_{\text{int}}^k|M_s} \tag{4}$$

where γ is the Gilbert gyromagnetic ratio, Ms is the saturation magnetization, H_{int}^k is the kth Fourier component of the mean demagnetizing field obtained for OOMMF micromagnetic simulations.

Fig. 4(a) shows the dispersion curves of SWs versus $P1$ with $P=16.5$ nm and Fig. 4(b) compares the gap width observed in the simulation to the results of the analytical calculation. The results demonstrate an excellent agreement between the numerically and analytically-computed gap widths. For $P1=7.5$ nm and $P1=9$ nm, the results of the analytical calculation differ by 1.3 GHz, or ~10%, from that of micromagnetic simulation.

Fig. 5 shows that the gap center of the first forbidden band can be regulated simply by changing the period P. According to the above discussions, the gap center and gap width of the forbidden band can be manipulated flexibly by changing both P and $P1/P$. This behavior can be exploited to enable the design of efficient SWs filters that reject SWs in a specific frequency band and pass all other frequencies. Fig. 5(b) shows four examples of such planar MCW,

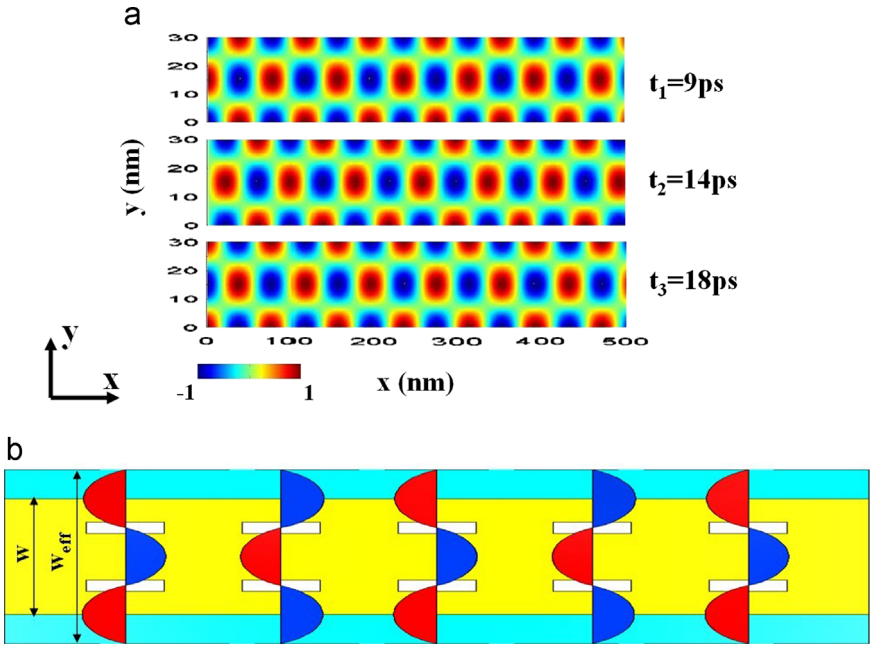

Fig. 3. (a) SWs spatial distribution profile obtained from the analytical form of Eq. (1) with different time. (b) Schematic SW mode ($m=3$) profiles. w is the geometrical width of strip, weff is the effective width of the strip, red indicates a high magnetization ($+z$) and blue reflects a low magnetization ($-z$). (For interpretation of the references to color in this figure legend, the reader is referred to the web version of this article.)

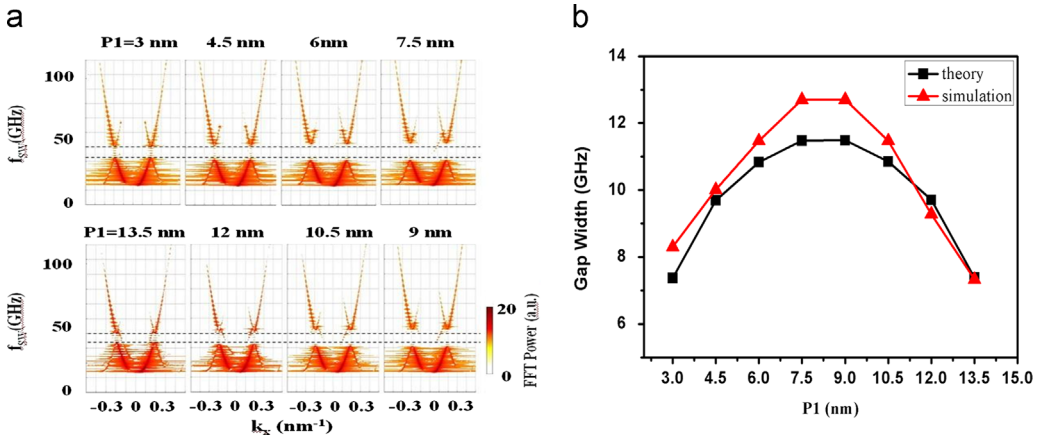

Fig. 4. (a) The dispersion curves of SWs with respect to P1 while maintaining $P=16.5$ nm. (b) The gap width obtained from micromagnetic simulation and analytical calculation.

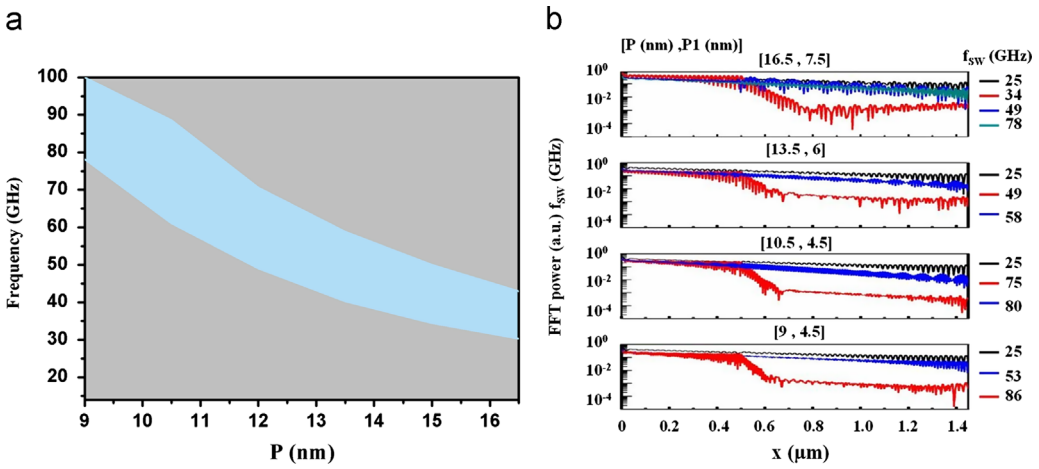

Fig. 5. (a) Band gap diagram with respect to P while maintaining $P1 \approx P2$. The gray region represents the allowed bands, while the blue region denotes the first forbidden band. (b) The FFT power profiles versus the propagation distance x for the indicated frequencies, are illustrated, respectively.

which were designed to reject only SWs within the frequency band $\Delta f_{SW}=30.3$–43 GHz, $\Delta f_{SW}=40.3$–59 GHz, $\Delta f_{SW}=61$–89 GHz and $\Delta f_{SW}=78$–100 GHz, respectively.

4. Conclusions

In conclusion, MCW with a single controllable magnonic band gap have been designed and analyzed both micromagnetically and through analytical calculations. The second forbidden band can be eliminated by adjusting the distance between two rectangular-shaped holes to half-wavelength of SWs in the y direction of MCW. Moreover, it can be found that the gap center and the gap width are controllable by the period P and the length of rectangular-shaped holes $P1$. MCW with a controllable single band gap provide a promising means for enabling SW-based signal transmission and processing devices in the gigahertz range.

Acknowledgments

This paper was supported by the National Nature Science Foundation of China under Grant nos. 61071028, 61271037, 51171038, 61271038 and 61021061.

References

[1] C. Kittel, Excitation of spin waves in a ferromagnet by a uniform rf field, Physical Review 110 (1958) 1295–1297.
[2] B.A. Kalinikos, A.N. Slavin, Theory of dipole-exchange spin wave spectrum for ferromagnetic films with mixed exchange boundary conditions, Journal of Physics C: Solid State Physics 19 (1986) 7013–7033.
[3] J.D. Adam, T.W. O'Keeffe, R.W. Patterson, Magnetostatic wave to exchange resonance coupling, Journal of Applied Physics 50 (2446) (1979).
[4] A.D. Fisher, J.N. Lee, E.S. Gaynor, A.B. Tveten, Optical guided-wave interactions with magnetostatic waves at microwave frequencies,, Applied Physics Letters 41 (1982) 779–781.
[5] K.-S. Lee, D.-S. Han, S.-K. Kim, Physical origin and generic control of magnonic band gaps of dipole-exchange spin waves in width-modulated nanostrip waveguides, Physical Review Letters 102 (2009) 127202-1–127202-4.
[6] S.-K. Kim, K.-S. Lee, D.-S. Han, A gigahertz-range spin-wave filter composed of width-modulated nanostrip magnonic-crystal waveguides, Applied Physics Letters 95 (2009) 082507-1–082507-3.
[7] F.S. Ma, H.S. Lim, Z.K. Wang, S.N. Piramanayagam, S.C. Ng, M.H. Kuok, Micromagnetic study of spin wave propagation in bicomponent magnonic crystal waveguides,, Applied Physics Letters 98 (2011) 153107-1–153107-3.
[8] F.S. Ma, H.S. Lim, Z.K. Wang, S.N. Piramanayagam, S.C. Ng, M.H. Kuok, Effect of interrow magnetic coupling on band structures of 2-D magnonic crystal waveguides, IEEE Transactions on Magnetics 47 (2011) 2689–2692.
[9] F.S. Ma, H.S. Lim, V.L. Zhang, Z.K. Wang, S.N. Piramanayagam, S.C. Ng, M. H. Kuok, Band structures of exchange spin waves in one-dimensional bi-component magnonic crystals, Journal of Applied Physics 111 (2012) 064326-1–064326-4.
[10] M.P. Kostylev, A.A. Serga, T. Schneider, B. Leven, B. Hillebrands, Spin-wave logical gates, Applied Physics Letters 87 (2005) 153501-1–153501-3.
[11] K.-S. Lee, S.-K. Kim, Conceptual design of spin wave logic gates based on a Mach–Zehnder-type spin wave interferometer for universal logic functions,, Journal of Applied Physics 104 (2008) 053909-1–053909-4.
[12] A. Khitum, D.E. Nikonov, M. Bao, K. Galatsis, K.L. Wang, Feasibility study of logic circuits with a spin wave bus,, Nanotechnology 18 (2007) 465202-1–465202-9.
[13] Y. Au, E. Ahmad, O. Dmytriiev, M. Dvornik, T. Davison, V.V. Kruglyak, Resonant microwave-to-spin-wave transducer,, Applied Physics Letters 100 (2012) 182404-1–182404-5.
[14] A.V. Chumak, P. Pirro, A.A. Serga, M.P. Kostylev, R.L. Stamps, H. Schultheiss, Spin-wave propagation in a microstructured magnonic crystal, Applied Physics Letters 95 (2009) 262508-1–262508-3.
[15] A.V. Chumak, T. Neumann, A.A. Serga, B. Hillebrands, M.P. kostylev, A current-controlled, dynamic magnonic crystal, Journal of Physics D: Applied Physics 42 (2009) 205005-1–205005-8.
[16] A version of the OOMMF code used is 1.2a4. See ⟨http://math.nist.gov/oommf⟩.
[17] D. Kumar, O. Dmytriiev, S. Ponraj, A. Barman, Numerical calculation of spin wave dispersions in magnetic nanostructures, Journal of Physics D: Applied Physics 45 (2012) 015001-1–015001-10.
[18] T.W. O'Keffe, R.W. Patterson, Magnetostatic surface-wave propagation in finite samples, Journal of Applied Physics 49 (1978) 4886–4895.
[19] J.D. Joannopoulos, R.D. Meade, J.N. Winn, Photonic Crystals: Molding the Flow of Light, 2nd ed, Princeton University, Princeton, HJ, 2008.
[20] The computational parameters as follows: $n=3$, $k_x^n=0.08$ nm^{-1}, $\omega=55$ GHz, and $\varphi_n=0$.
[21] K.Yu. Guslienko, S.O. Demokritov, B. Hillebrands, A.N. Slavin, Effective dipolar boundary conditions for dynamic magnetization in thin magnetic stripes, Physical Review B 66 (2002) 132402-1–132402-4.
[22] K. Yu Guslienko, A.N. Slavin, Boundary conditions for magnetization in magnetic nonoelements, Physical Review B 72 (2005) 014463-1–014463-4.
[23] C. Kittel, Introduction to Solid State Physics, 7th ed., John Wiley & Sons, Inc., NY, 1996.
[24] R. Zivieri, S. Tacchi, F. Montoncello, L. Giovannini, F. Nizzoli, M. Madami, G. Gubbiotti, Bragg diffraction of spin waves from a two-dimensional antidot lattice, Physical Review B 85 (2012) 012403-1–012403-6.